

Lawrence Berkeley National Laboratory

LBL Publications

Title

Preliminary experimental comparison and feasibility analysis of CO₂/R134a mixture in Organic Rankine Cycle for waste heat recovery from diesel engines

Permalink

<https://escholarship.org/uc/item/8kd4h9vr>

Authors

Liu, Peng

Shu, Gequn

Tian, Hua

et al.

Publication Date

2019-10-01

DOI

10.1016/j.enconman.2019.111776

Peer reviewed

1 **Preliminary experimental comparison and**
2 **feasibility analysis of CO₂/R134a mixture in**
3 **Organic Rankine Cycle for waste heat recovery**
4 **from diesel engines**

5 **Peng Liu^{a,b}, Gequn Shu^{a,*}, Hua Tian^{a,*}, Wei Feng^b, Lingfeng**
6 **Shi^a, Zhiqiang Xu^a**

7 ^aState Key Laboratory of Engines, Tianjin University, 92 Weijin Road,
8 Nankai District, Tianjin 300072, China

9 ^bEnergy Technologies Area, Lawrence Berkeley National Laboratory,
10 1 Cyclotron Road, Berkeley, CA 94720, USA

11 * Corresponding author.

12 Tel: +86 22-27409558

13 E-mail: sgq@tju.edu.cn (G. Shu), thtju@tju.edu.cn (H. Tian)

14 **Abstract**

15 This paper presents results of a preliminary experimental study
16 of the Organic Rankine Cycle (ORC) using CO₂/R134a mixture based
17 on an expansion valve. The goal of the research was to examine the
18 feasibility and effectiveness of using CO₂ mixtures to improve
19 system performance and expand the range of condensation
20 temperature for ORC system. The mixture of CO₂/R134a (0.6/0.4) on
21 a mass basis was selected for comparison with pure CO₂ in both the
22 preheating ORC (P-ORC) and the preheating regenerative ORC (PR-
23 ORC). Then, the feasibility and application potential of CO₂/R134a
24 (0.6/0.4) mixture for waste heat recovery from engines was tested
25 under ambient cooling conditions. Preliminary experimental results
26 using an expansion valve indicate that CO₂/R134a (0.6/0.4) mixture
27 exhibits better system performance than pure CO₂. For PR-ORC
28 using CO₂/R134a (0.6/0.4) mixture, assuming a turbine isentropic
29 efficiency of 0.7, the net power output estimation, thermal efficiency
30 and exergy efficiency reached up to 5.30kW, 10.14% and 24.34%,
31 respectively. For the fitting value at an expansion inlet pressure of
32 10MPa, the net power output estimation, thermal efficiency and
33 exergy efficiency using CO₂/R134a (0.6/0.4) mixture achieved
34 increases of 23.3%, 16.4% and 23.7%, respectively, versus results
35 using pure CO₂ as the working fluid. Finally, experiments showed
36 that the ORC system using CO₂/R134a (0.6/0.4) mixture is capable of
37 operating stably under ambient cooling conditions (25.2~31.5°C),
38 demonstrating that CO₂/R134a mixture can expand the range of

39 condensation temperature and alleviate the low-temperature
40 condensation issue encountered with CO₂. Given Under the ambient
41 cooling source, it is expected that ORC using CO₂/R134a (0.6/0.4)
42 mixture will improve the thermal efficiency of a diesel engine by
43 1.9%.

44

45 **Keywords:** CO₂/R134a mixture; experimental comparison;
46 feasibility analysis; Organic Rankine Cycle; engine waste heat
47 recovery

48

49 **1. Introduction**

50 World Energy Outlook in 2017 reported that China may become
51 the world's largest oil importer in 2020 [1]. A major obstacle to
52 reducing China's oil consumption is the growing demand of crude oil
53 in the transportation sector. The crude oil consumed by internal
54 combustion engines (ICEs) accounts for 60% of China's total crude
55 oil consumption [1]. Constrained by the structure of the ICE and the
56 Carnot cycle efficiency, more than half of the combustion heat of an
57 internal combustion engine is discharged through various forms of
58 waste heat. Hence, waste heat recovery (WHR) technologies are
59 regarded as a promising way to improve the fuel efficiency of ICEs
60 and thus to reduce China's oil consumption. Among technologies,
61 Organic Rankine Cycle (ORC) is considered suitable for ICE-WHR
62 because of its high efficiency, suitable system size and low impact
63 on the ICE itself [2].

64 The choice of working fluid is critical for using an ORC system
65 for ICE-WHR. Recent research has examined traditional refrigerant-
66 based ORC systems in terms of integration optimization [3],
67 selection of working fluid [4], configuration comparison [5] and
68 dynamic performance [6]. However, traditional refrigerants,
69 including CFCs, HCFCs and HFCs, contribute significantly to climate
70 change and global warming [7]. The global warming potential (GWP)
71 and ozone depletion potential (ODP) of such refrigerants are higher
72 than those of CO₂. Various protocols and amendments have been
73 established to control and limit the use and production of traditional
74 refrigerants. Recently, governments around the world introduced a
75 phase-out plan for CFCs and HCFCs and use limitations for HFCs [8].
76 It is important, therefore, to investigate alternative working fluids
77 that have zero GWP and ODP.

78 This paper is organized as follows: A literature review is
79 presented in Section 2. Section 3 gives a brief description of the
80 ORC test bench used in the current study. Section 4 discusses the
81 selection of working fluids. The experimental strategy is presented

3

4

82 in Section 5. Section 6 describes the experiments conducted to
83 compare performance of working fluids and to perform feasibility
84 analysis. Major conclusions are summarized at the end of the paper.
85 The originality of this paper centers on three primary features.

- 86 1. This paper presents the first experimental results for an ORC
87 system that uses CO₂/R134a mixture.
- 88 2. This paper describes the first attempt to conduct an
89 experimental comparison between a CO₂/R134a mixture and
90 pure CO₂ in an ORC system and to demonstrate the
91 performance improvement obtained by CO₂/R134a mixture.
- 92 3. Experimental results under ambient cooling conditions
93 indicate that CO₂/R134a mixture can expand the range of
94 condensation temperatures and alleviate the issue of the
95 low-temperature condensation encountered with CO₂.

96 **2. Literature review**

97 In several earlier investigations of ORC-based ICE-WHR, the CO₂
98 transcritical Rankine cycle (TRC) showed great potential [9-11]. First,
99 CO₂ is environmentally friendly, non-toxic, non-flammable and
100 inexpensive. In addition, CO₂ provides heat stability adequate to
101 withstand the high temperatures of the exhaust gas from ICEs.
102 Secondly, previous studies indicated that CO₂ is capable of utilizing
103 heat from exhaust gas and engine coolant simultaneously and has a
104 good thermal matching, reducing irreversible losses occurred during
105 the heating process [9, 12]. Finally, CO₂ supports the miniaturization
106 of ORC systems: CO₂ turbines are expected to be small and simple,
107 and CO₂ holds promise for use with compact microchannel heat
108 exchangers [13, 14]. Byung Chul Choi [15] presented a CO₂-TRC with
109 two-stage reheat to recover waste heat from the jacket water and
110 the intercooler, revealing that the maximum cycle efficiency is
111 9.26%. Wang et al. [16] compared three configurations of CO₂ based
112 TRC concluding that the single stage cycle is preferable when the
113 exhaust gas temperature is 300 °C ~600 °C. Experimental analysis
114 conducted by the Echogen Power Company [17] indicated that CO₂-
115 based TRC achieved higher efficiency than organic or steam-based
116 Rankine cycle within a wide temperature range and for a small
117 system. Previous experiments conducted by our group
118 demonstrated that CO₂ based TRC could not only improve the
119 thermal efficiency and reduce the cooling load of the diesel
120 engine[11], but also possesses good dynamic characteristics [18-
121 20].

122 Because of the low critical temperature, however, it is difficult
123 for CO₂ to be condensed into a liquid state under the ambient
124 cooling conditions. This difficulty presents an obstacle to the

125 practical application of a CO₂ based TRC, especially for WHR for
126 vehicles. Meanwhile, CO₂ based TRC provides relatively low thermal
127 efficiency because of the corresponding small pressure ratio. To
128 alleviate the disadvantages noted above, some researchers have
129 explored the feasibility of using CO₂ mixtures[21-25]. Shu et al. [22]
130 investigated the performance improvement by using CO₂ mixture in
131 transcritical Rankine cycle for WHR of a diesel engine. The results
132 indicated that CO₂ mixture can improve system performance,
133 expand the range of condensation temperature and decrease
134 operating pressure. Dai et al. [23] studied the seven CO₂ mixtures in
135 low temperature TRC, revealing that such mixtures are capable of
136 improving thermal efficiency and reducing operating pressure in
137 comparison of CO₂. Wu et al. [24] compared various CO₂-based
138 mixtures for the energy conversion of geothermal water,
139 demonstrating that CO₂-based mixtures achieve superior thermo-
140 economic performance although they require a larger heat transfer
141 area. Yin et al. [26] investigated the supercritical/transcritical
142 Rankine cycle for geothermal power plants, using a CO₂/SF₆ mixture
143 and determining the optimal concentration of SF₆.

144 Despite some previous research, there are few reported
145 experiments that incorporate CO₂ mixtures into ORC. Indeed,
146 published results of ORC experiments using a CO₂ mixture as the
147 working fluid are extremely rare because of safety concerns,
148 insufficient experience and industrial confidentiality[27]. Wang et al.
149 [28] presented an experimental study of a low-temperature solar
150 ORC using R245fa/R152a mixture as working fluid, indicating that
151 R245fa/R152a mixture showed the potential to improve overall
152 efficiency. An experimental comparison between the R245fa/R134a
153 mixture and pure R245fa in a low-temperature small-scale ORC was
154 conducted by Bamorovat Abadi et al. [29]. The results showed that
155 R245fa/R134a mixture performed well with heat source
156 temperatures ranging from 80 °C to 100 °C and the mixture
157 achieved higher power output at a lower pressure ratio. Jung et al.
158 [30] used an ORC test rig to examine the dynamic behavior of
159 R245fa/R356mfc. Li et al. [31] conducted a performance comparison
160 between R245fa and a R245fa/R601a mixture in the ORC system
161 and concluding that the R245fa/R601a mixture improved the heat
162 transfer performance of the vapor generator and obtained higher
163 thermal efficiency. Pang et al. [32] examined the maximum net
164 power output of an ORC system for industrial waste heat using
165 R245fa, R123 and their mixtures.

166 Our literature review revealed that previous experimental
167 research into using CO₂ mixtures for ORC focused primarily on the
168 refrigerant/refrigerant mixtures, which have contributed to the

169 application of low-temperature ORC. Lacking are experimental
170 results for CO₂ mixtures in high-temperature ORC applications. In
171 addition, there are almost no experimental results to assess the
172 feasibility of using CO₂/R134a mixtures to expand the range of
173 condensation temperatures, which is required for using ICE-WHR in
174 vehicles.

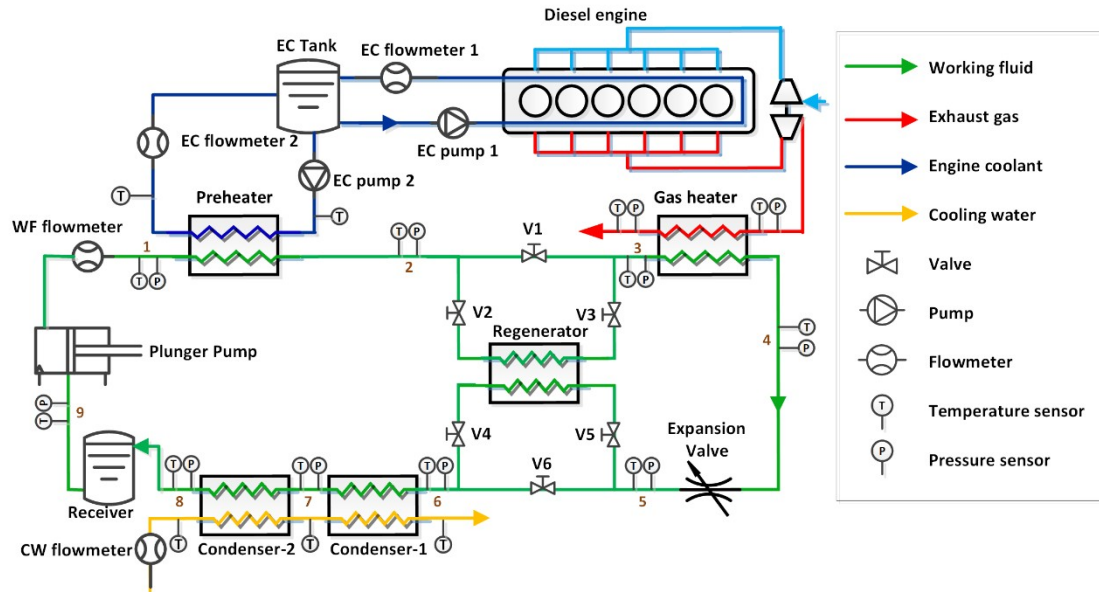
175 This paper describes a preliminary experimental study using an
176 expansion valve in a small-scale ORC test bench coupled with a
177 heavy-duty diesel engine. Exhaust gas and engine coolant were
178 utilized as heat sources for the ORC test bench. Measured operating
179 parameters as well as system performance of pure CO₂ and a
180 CO₂/R134a mixture (0.6/0.4 on a mass basis) were compared under
181 both a P-ORC and a PR-ORC. System performance using a CO₂/R134a
182 mixture under ambient cooling conditions also was analyzed.

183 **3. Description of test bench**

184 A small-scale Organic Rankine Cycle (ORC) test bench was built
185 to recover waste heat from the exhaust gas and engine coolant of a
186 diesel engine. The entire test bench comprises the diesel engine,
187 the ORC system and the cooling system. Measurement devices
188 including pressure transmitter, thermocouple and flow transmitter
189 are installed in the test bench. Fig.1 presents a schematic diagram
190 of the ORC test bench and indicates the location of each
191 measurement point. Fig.2 is a photo of the ORC test bench.

192 The engine used in the experiment is a heavy duty, 6-cylinder,
193 4-stroke diesel engine (parameters are detailed in Table 1). The
194 diesel engine is equipped with a system that can be used to control
195 and record the diesel engine's operating conditions. A water tank is
196 provided in lab to supply engine coolant for the diesel engine, and
197 the flow rate of engine coolant is controlled by pump (EC Pump 1 in
198 Fig.1). Another engine coolant pump (EC Pump 2 in Fig.1) is installed
199 to drive part of the engine coolant as the preheating source for the
200 ORC system.

201
202



203

204 **Fig.1.** Schematic diagram of the ORC test bench and the location of
 205 each measurement point.

206

207 **Table 1**

208 Specifications for diesel engine in test bench.

Parameter	Units	Description
Engine Type	-	In-line, 4 stroke
Cylinder number	-	6
Bore×Stroke	mm×mm	113×140
Displacement	L	8.424
Intake model	-	Supercharged and intercooling
Fuel injection	-	High pressure common rail
Maximum torque	N·m	1280@1200~1700rpm
Rated Speed	rpm	2200
Rated power	kW	243

209

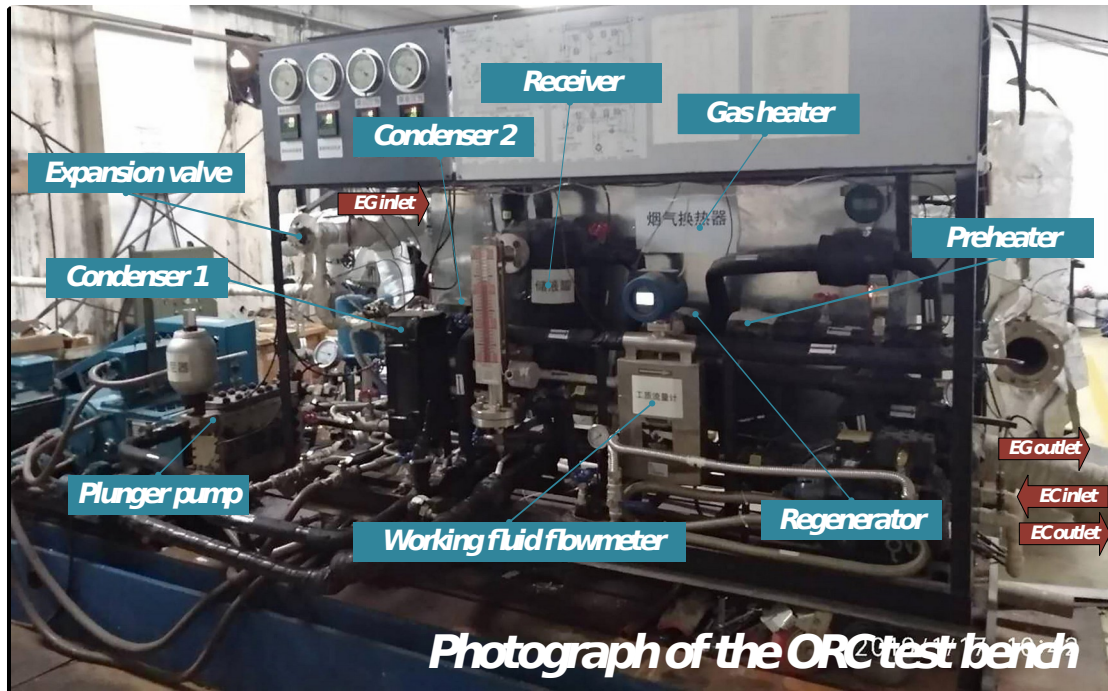


Fig.2. Photograph of the ORC test bench

210

211

212

213

214

215

216

217

218

219

220

221

222

223

224

225

226

227

228

229

230

231

232

233

234

235

236

237

The cooling system provides a steady cooling water source (5 °C -12°C) for the ORC system. Most of the cooling water is used to cool the working fluid in the condenser to ensure that it is in a liquid state when it flows into the liquid receiver. To prevent possible gasification of the working fluid during pressurization of the working fluid plunger pump, another small portion of the cooling water is used to cool the plunger pump head and the liquid receiver.

The ORC system consists of the preheater, regenerator, gas heater, expansion valve, control valves, condenser-1, condenser-2, plunger pump and some measurement devices. A self-made double-pipe type heat exchanger is used for the gas heater, since it must withstand both high temperature and high pressure. Brazed plate heat exchangers, supplied by SWEF, is used for the preheater, the regenerator and the condensers, considering the system compactness. The flow rate of the working fluid for the ORC system is controlled by a reciprocating plunger pump (model 3RC50A-1.7/12). The liquid receiver is designed and manufactured as a vertical cylindrical barrel with a volume of 10L. A magnetic flip plate type level sensor installed in the liquid receiver shows the change of liquid height in the receiver. There is a lack of corresponding experiment results about CO₂ mixture, considering the possible turbine damage caused by the refrigerant component in CO₂/R134a mixture, a home-made expander valve is temporarily used to replace the expander in the current studies. By controlling the opening degree of the expander valve, we can estimate and analyze

13

14

238 system performance under various expansion inlet pressures.

239 The experimental bench is unique in that the preheating ORC (P-
 240 ORC) system and preheating regenerative ORC (PR-ORC) system can
 241 easily be switched by controlling valves 1 through 6. Closing valves
 242 2 through 5 and opening valves 1 and 6 imitates a P-ORC system.
 243 Conversely, closing valves 1 and 6 and opening valves 2 through 5
 244 imitates a PR-ORC system.

245 Measuring instruments such as pressure sensors, temperature
 246 sensors and flow meters are installed on the test bench, as shown in
 247 Fig.1. A data collection module performs data acquisition and
 248 conversion, then connects to a computer through an RS232
 249 communication cable. The overall performance of the system can be
 250 determined by measuring the thermodynamic states at each
 251 measurement point. Using the error analysis method described in
 252 our previous publication [18], the maximum relative uncertainties of
 253 $Q_{gh,f}$, $Q_{gh,eg}$ and $Q_{con,cw}$ are 1.1%, 5.71% and 2.0%, respectively.
 254 Specifications and uncertainties of measuring devices are listed in
 255 Table. 2.

256

257 **Table 2**

258 Specifications and accuracies of the test bench measuring devices.

Measuring device	Type	Range	Accuracy
Flow rate			
Engine intake air flowmeter	Laminar flow	0~1350 kg/h	±0.5%
Fuel consumption meter	-	5~2000k g/h	-
CO ₂ flowmeter	Coriolis type	0~1080 kg/h	±0.2%
EC flowmeter1	Turbine	2~40 m ³ /h	±0.5%
EC flowmeter2	Turbine	0~10 m ³ /h	±0.5%
Cooling water flowmeter	Turbine	0~12 m ³ /h	±1%
Liquid level			
CO ₂ liquid level meter	Magnetic flap type	0~30cm	±3.3%
Temperature			
Temperature sensor for EG	Thermocouple type	60~650 ^o C	±1%

Temperature sensor for others	Thermo-resistive type	-200~500 °C	±0.15 %
Pressure			
Pressure transmitter for EG and CW	Low pressure type	0~0.5 MPa	±0.065 %
Pressure transmitter for low pressure CO ₂	Low pressure type	0~12 MPa	±0.065 %
Pressure transmitter for high pressure CO ₂	High pressure type	0~14 MPa	±0.065 %

259

260 4. Selection of Working fluid

261 Previous studies have analyzed and discussed the theoretical
 262 thermodynamic performance of the ORC using mixtures composed
 263 of CO₂ and other refrigerants. To allow for condensation at ambient
 264 temperatures in practical applications, the refrigerant additive
 265 should have a higher critical temperature than CO₂. Moreover, the
 266 refrigerant additive should have good safety and environmental
 267 characteristics. Because it is non-flammable, has zero ODP and a
 268 low GWP, R134a is widely used as a high-temperature refrigerant in
 269 automobile air conditioners[33], which indicate R134a hold great
 270 potential to be used for other application in automobile field.
 271 Previous theoretical analysis conducted by our group [22] showed
 272 that CO₂/R134a mixture has moderate temperature glide and good
 273 thermodynamic performance. Ref. [22] also concludes that
 274 CO₂/R134a mixture with an approximate 40%~50% mass fraction of
 275 R134a may produce superior system performance. Thus, we
 276 selected the mixture of CO₂/R134a (0.6/0.4) on a mass basis for
 277 comparison with pure CO₂. The major physical parameters of pure
 278 CO₂, R134a and CO₂/R134a mixture are listed in Table 3. Fig.3 shows
 279 the *T-s* diagram of CO₂/R134a (0.6/0.4) mixture and pure CO₂. It is
 280 clear that CO₂/R134a (0.6/0.4) mixture owns higher critical
 281 temperature and critical pressure in comparison with CO₂. It should
 282 be noted that the thermodynamic properties of the working fluid
 283 were obtained using REFPROP 9.0.

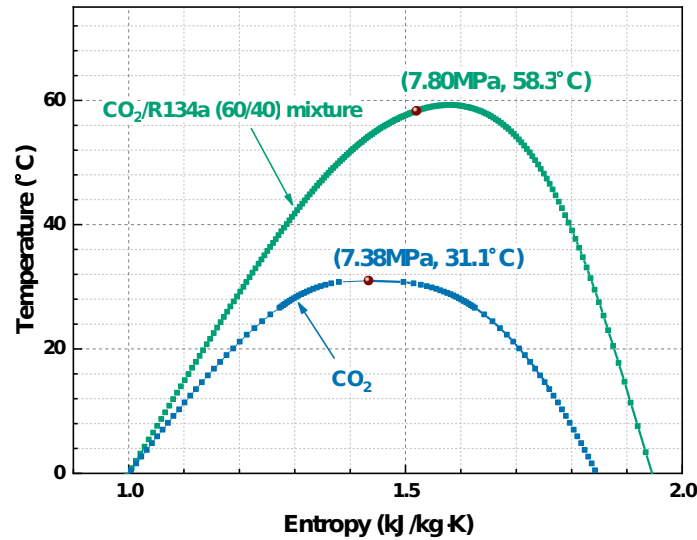
284 **Table 3**

285 Properties of CO₂, R134a and CO₂/R134a (0.6/0.4) mixture.

	CO ₂	R134a	CO ₂ /R134a (0.6/0.4)
Molecular mass (g/mol)	44.01	102.03	67.22
Critical temperature (°C)	31.1	101.1	58.3
Critical pressure (MPa)	7.38	4.06	7.80

ODP	0	0	-
GWP	1	1300	-
ASHRAE 34 safety group	A1	A1	-

286



287

288 **Fig.3.** T-s diagram of CO₂/R134a (0.6/0.4) mixture and pure CO₂.

289 **5. Experimental strategy and evaluation model**

290 **5.1 Experimental strategy**

291 This paper describes the experimental approach in two parts.
 292 First, the performance of the CO₂/R134a mixture is evaluated and
 293 compared with that of pure CO₂ in the P-ORC and PR-ORC. Then,
 294 after shutting down the refrigerating unit, another experimental test
 295 is conducted under ambient cooling conditions to demonstrate the
 296 feasibility and potential of the CO₂/R134a mixture for waste heat
 297 recovery from vehicle engines.

298 To perform a reasonable comparison between pure CO₂ and the
 299 CO₂/R134a mixture, the diesel engine operates under the same
 300 working conditions for both (50% load at 1100rpm), which is the
 301 medium duty of the diesel engine used in the test. Even if the diesel
 302 engine runs at a constant operating point, clearly the temperature
 303 and flow rate of waste heat sources may fluctuate in response to
 304 factors such as changes in environmental conditions or unsteady
 305 engine operation. Table 4 shows the operating parameters and
 306 waste heat source parameters for the diesel engine used in the
 307 experiments, as well as the maximum relative difference (RD_{max}) of
 308 each parameter. The maximum relative differences are obtained
 309 based on the engine coolant flow rate due to fluctuations in the

310 level of liquid in the water tank. Except for the engine coolant flow
 311 rate, the maximum relative differences of parameters are within 5%.
 312 The difference in heat sources caused by the unsteady operation of
 313 the diesel engine is acceptable in this comparative experiment.

314

315 **Table 4**

316 Engine operating parameters and heat source conditions for various
 317 experimental scenarios and maximum relative differences of
 318 parameters.

Parameter	Pure CO ₂		CO ₂ /R134a mixture		RD _{max} x
	P-ORC	PR-ORC	P-ORC	PR-ORC	
Engine speed (rpm)	1100	1106	1099	1098	0.5%
Engine torque (N·m)	594	603	601	601	1.0%
Power output (kW)	68.2	69.7	68.8	68.8	1.2%
BSFC (g/kWh)	215.2	228.2	221.8	221.8	3.0%
Exhaust gas temperature (°C)	489.3~50	490.6~50	490.7~49	494.4~49	2.1%
Exhaust gas mass flow rate (kg/h)	1.0	6.6	3.7	6.0	
Engine coolant temperature (°C)	320.6~32	316.0~32	325.6~32	323.9~32	2.1%
Engine coolant mass flow rate (m ³ /h)	3.4	1.1	8.5	6.2	
Engine coolant temperature (°C)	71.3~75.	71.3~72.	69.9~73.	70.8~73.	5.0%
Engine coolant mass flow rate (m ³ /h)	7	3	5	4	
Engine coolant mass flow rate (m ³ /h)	0.23~0.2	0.24~0.2	0.23~0.2	0.24~0.2	10.2%
Engine coolant mass flow rate (m ³ /h)	4	5	7	6	%

319 $RD_{max} = |X - X_{ave}|_{max} / X_{ave}$

320

321 Experimental strategy is described briefly here. First, some
 322 preparation work must be done, such as checking the seals in the
 323 ORC bench and verifying the position of valves and the functioning
 324 of refrigeration unit. Then, the diesel engine is started and warmed
 325 up. Testing with the ORC test bench begins when the temperature of
 326 the exhaust gas reaches 180 °C. The speed and load of the diesel
 327 engine as well as the mass flow rate of the working fluid are
 328 increased gradually to their set points. As mentioned above, the set
 329 operating conditions of the diesel engine are 600 N·m and 1100
 330 rpm. The flow rate of the working fluid is set to 11.5±0.2kg/min.
 331 After the diesel engine and the ORC test bench are operating
 332 consistently, the expansion valve opening is reduced manually to
 333 create sub-scenarios involving various pressures on ORC system.
 334 This way, the system performance of pure CO₂ and of CO₂/R134a
 335 mixture can be compared preliminarily under various pressures.

336 During the experimental process, for safety reasons the maximum
 337 pressure of the ORC test bench cannot exceed 11 MPa. It should be
 338 noted that those experiments were performed at different time, so
 339 that the temperatures of the cooling water differed slightly because
 340 it was affected by the ambient temperature. Table 5 gives the
 341 cooling conditions for the various tests.

342 **Table 5**

343 Cooling conditions for different working fluids and modes.

	Pure CO ₂		CO ₂ /R134a mixture	
	P-ORC	PR-ORC	P-ORC	PR-ORC
Cooling water temperature (°C)	7.6~7.8	7.1~7.9	9.4~9.5	9.4~9.4
Cooling water mass flow rate (m ³ /h)	1.87~1.89	1.93~1.94	1.92~1.93	1.92~1.92

344 5.2 Evaluation model

345 Based on the measured parameters, we estimated the
 346 thermodynamic performance of the system, including net output
 347 work, thermal efficiency and exergy efficiency. MATLAB 2015
 348 software was used to establish the mathematic models. The
 349 mathematical equations for each component and for system
 350 performance are described below.

351 The amount of heat absorbed by the working fluid during the
 352 heating process—in the preheater, the regenerator and the gas
 353 heater—can be calculated as follows.

$$354 \quad \dot{Q}_{pre} = \dot{m}_f (h_2 - h_1) \quad (1)$$

$$355 \quad \dot{Q}_{reg} = \dot{m}_f (h_3 - h_2) \quad (2)$$

$$356 \quad \dot{Q}_{gh} = \dot{m}_f (h_4 - h_3) \quad (3)$$

357 Because the radial flow turbine is unfinished, in the test bench
 358 the expansion valve is used temporarily in place of the expander.
 359 With the measured parameters of expansion inlet temperature,
 360 expansion inlet pressure and expansion outlet pressure, the net
 361 power output can be estimated by assuming a constant isentropic
 362 expansion efficiency as follows [11, 34].

$$363 \quad \dot{W}_p = \dot{m}_f (h_1 - h_5) \quad (4)$$

$$364 \quad \dot{W}_{exp,est} = \dot{m}_f (h_4 - h_5) \quad (5)$$

$$365 \quad h_5 = h_4 - (h_4 - h_{5,ideal}) \eta_{exp} \quad (6)$$

366
$$\dot{W}_{net,est} = \dot{W}_{exp,est} - \dot{W}_p \quad (7)$$

367 wherein $h_{5,ideal}$ is the ideal enthalpy of state 5, assuming that the
 368 working fluid expands from state 4 to state 5 in an isentropic
 369 process. h_5 is the enthalpy at state 5 with the consideration of
 370 irreversible loss in expansion process. The isentropic efficiency of
 371 the expander is assumed to be 70%, which is the target value when
 372 manufacturing turbine and also is reasonable for current CO₂ power
 373 cycle applications [35].

374 The thermal efficiency of the ORC system is defined as follows.

375
$$\eta_{th} = \frac{\dot{W}_{net,est}}{\dot{Q}_{pre} + \dot{Q}_{gh}} \quad (8)$$

376 The exergy destruction in each heat exchanger and the exergy
 377 efficiency are calculated by:

378
$$\dot{i}_{pre} = (\dot{E}_{EC,in} - \dot{E}_{EC,out}) - (\dot{E}_2 - \dot{E}_1) \quad (9)$$

379
$$\dot{i}_{reg} = (\dot{E}_5 - \dot{E}_6) - (\dot{E}_3 - \dot{E}_2) \quad (10)$$

380
$$\dot{i}_{gh} = (\dot{E}_{EG,in} - \dot{E}_{EG,out}) - (\dot{E}_4 - \dot{E}_3) \quad (11)$$

381
$$\dot{i}_{con1+con2} = (\dot{E}_6 - \dot{E}_8) \quad (12)$$

382
$$\eta_{ex} = \frac{\dot{W}_{net,est}}{(\dot{E}_{EC,in} - \dot{E}_{EC,out}) + (\dot{E}_{EG,in} - \dot{E}_{EG,out})} \quad (13)$$

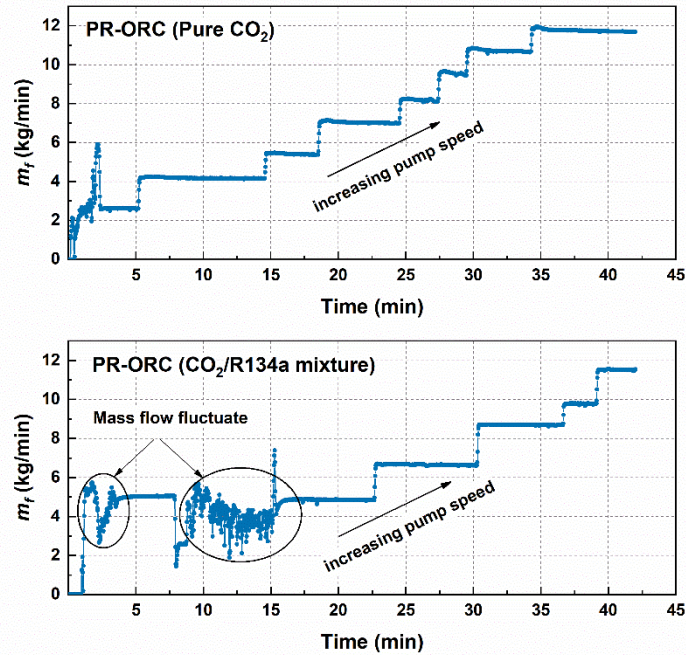
383 6. Results and discussion

384 During the experiments, the measured parameters, including
 385 temperature, pressure and flow rate at each measurement point,
 386 are recorded automatically. Before evaluating system performance,
 387 we compared the measured operating parameters between pure
 388 CO₂ and CO₂/R134a mixture. Subsequently, system thermodynamic
 389 performance was discussed.

390 6.1 Comparison of operating parameters of pure 391 CO₂ and CO₂/R134a mixture

392 At the beginning of the experiment, the flow rate of the working
 393 fluid flow rate was gradually increased to the set value. This process
 394 took about 40 minutes. The data collected for pure CO₂ and
 395 CO₂/R134a mixture are shown in Fig.4. As noted, the CO₂ flow rate
 396 was increased steadily after the period of flow fluctuation when the
 397 working fluid pump started. However, the ORC system using

398 CO₂/R134a mixture underwent drastic flow fluctuations over a long
 399 period, which could be caused by the unevenness of the mixture.
 400 After the CO₂/R134a mixture mixed evenly, the flow rate remained
 401 consistent throughout the experiment. Hence, preparation work is
 402 recommended to ensure complete mixing of CO₂/R134a mixture
 403 when used as the working fluid of an ORC.

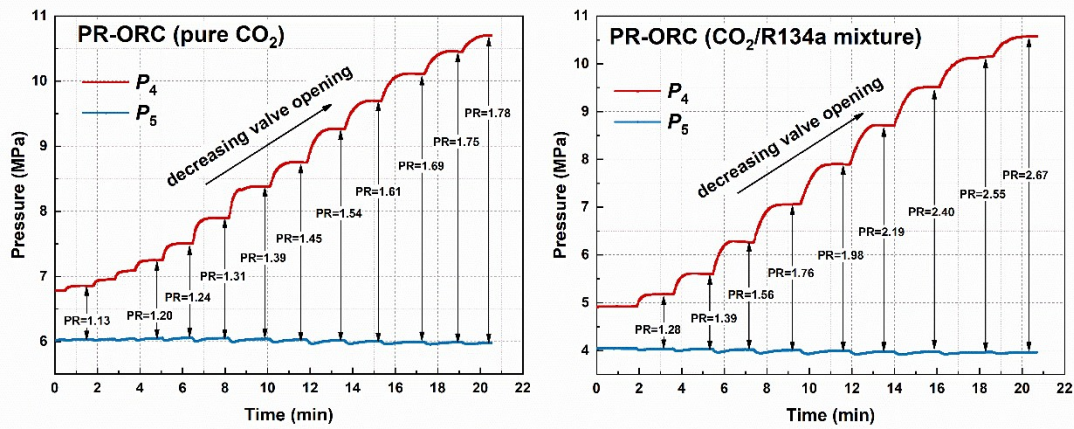


404
 405 **Fig.4.** Variation in flow rate of the working fluid at the beginning of
 406 experiment.
 407

408 Tests were begun after the ORC test bench and diesel engine
 409 operated steadily. Fig.5 shows the variation of expansion inlet and
 410 outlet pressures over time for the PR-ORC system. Each step change
 411 of pressure means a decrease in valve opening. For pure CO₂, 11
 412 steady operating points, corresponding to expansion inlet pressures
 413 ranging from 6.8 to 10.7 MPa, were selected for analysis and
 414 comparison. 9 steady operating points, corresponding to expansion
 415 inlet pressures ranging from 5.2 to 10.6 MPa, were chosen for
 416 CO₂/R134a mixture. As shown in Fig.5, the expansion outlet pressure
 417 when using CO₂/R134a mixture is significantly lower than that when
 418 using pure CO₂. This difference is attributable to the fact that
 419 CO₂/R134a mixture exhibits a lower saturated pressure than pure
 420 CO₂ at the same temperature. As a consequence, the pressure ratios
 421 of CO₂/R134a mixture are larger than those of pure CO₂, which also
 422 are noted in Fig. 5.

423 Expansion inlet pressure was selected as the indicator for
 424 detecting steady state in an ORC system[18]. As shown in Fig. 5, the
 425 entire ORC system operates steadily within 2~3min before the

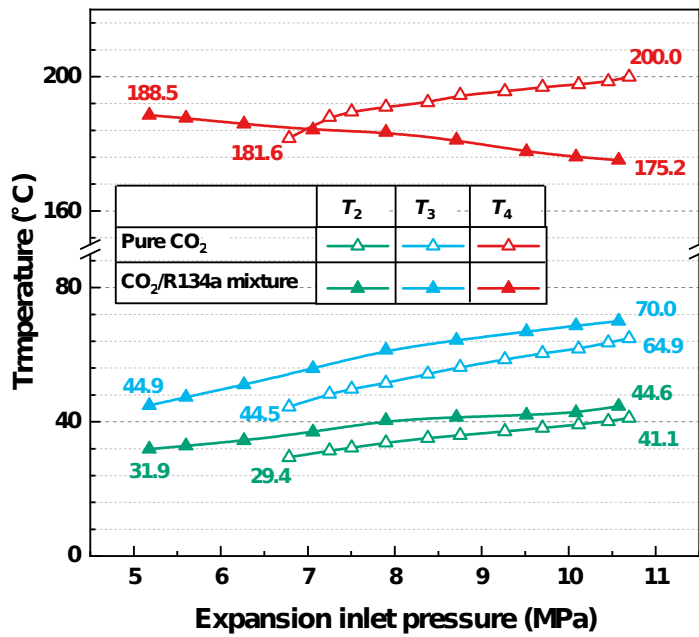
426 expansion valve opening is changed again. Steady state points
 427 within 20s before the next change of expansion valve are used for
 428 performance analysis.



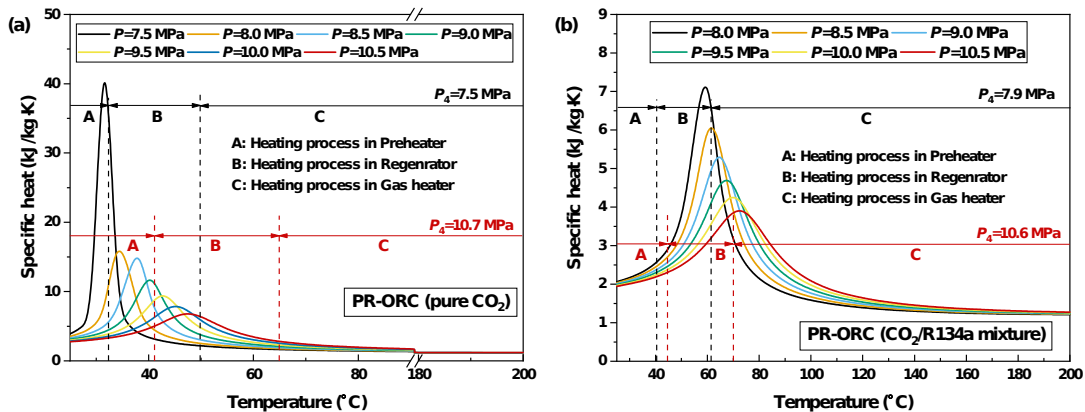
429

430 **Fig. 5.** Variation in expansion inlet and outlet pressures over time
 431 for the PR-ORC.
 432

433 Temperature variation at each measurement point directly
 434 reflects the heat recovery capacity of an ORC system. Fig. 6 shows
 435 the variation in temperature with expansion inlet pressure at the
 436 preheater outlet (T_2), the regenerator outlet (T_3) and the gas heater
 437 outlet (T_4). For both pure CO_2 and $\text{CO}_2/\text{R134a}$ mixture, T_2 and T_3
 438 demonstrate a trend of increasing with expansion inlet pressure.
 439 Meanwhile, the temperatures of pure CO_2 at points 2 and 3 are
 440 always lower than those of $\text{CO}_2/\text{R134a}$ mixture. This finding can be
 441 explained by the fact that pure CO_2 is capable of absorbing more
 442 heat per mass at low-medium temperatures, reflected by larger
 443 specific heat capacity, as shown in Fig.7. A further finding is that as
 444 the expansion inlet pressure increases, the T_4 for CO_2 increases from
 445 181.6°C to about 200°C , while the T_4 of $\text{CO}_2/\text{R134a}$ mixture
 446 decreases from 188.5°C to 175.2°C . The reversed temperature
 447 trends for pure CO_2 and $\text{CO}_2/\text{R134a}$ mixture result from the
 448 combination of two actions: (a) the mass flow rate of the working
 449 fluid decreases due to the throttle effect of the expansion valve,
 450 producing the increase in T_4 for both CO_2 and the $\text{CO}_2/\text{R134a}$
 451 mixture; and (b) the specific heat of the $\text{CO}_2/\text{R134a}$ mixture in the
 452 exhaust gas recovery zone increases with pressure (Fig. 7(b)),
 453 indicating that the $\text{CO}_2/\text{R134a}$ mixture can absorb more heat per
 454 mass than can pure CO_2 . A greater capacity for heat absorption
 455 results in the decrease in T_4 . Conversely, no sensible change in
 456 specific heat in the exhaust gas recovery zone was seen for CO_2 (Fig.
 457 7(a)).



458
459 **Fig. 6.** Variation in temperature at the preheater outlet (T_2),
460 regenerator outlet (T_3) and gas heater outlet (T_4) with expansion
461 inlet pressure.
462

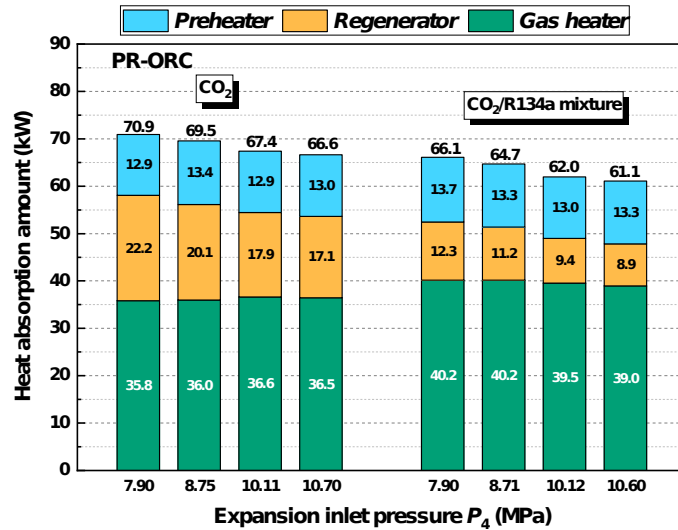


463
464 **Fig. 7.** Variation in specific heat capacity under various pressures.
465 (a) pure CO₂; (b) CO₂/R134a mixture.

466 6.2 Comparison of the performance of pure CO₂ and 467 CO₂/R134a mixture

468 The aim of this section is to examine and compare the system
469 performance of pure CO₂ and CO₂/R134a (0.6/0.4) mixture in an ORC
470 system. First, we discuss the difference in the capacity for waste
471 heat recovery. Fig. 8 shows the amount of heat absorption for pure
472 CO₂ and CO₂/R134a mixture in the PR-ORC system. On the whole,

473 pure CO₂ is capable of absorbing more heat than CO₂/R134a
 474 mixture. Compared to pure CO₂, CO₂/R134a mixture recovers more
 475 heat from the exhaust gas, which is attributed to the high c_p in the
 476 exhaust gas recovery zone of CO₂/R134a mixture (as shown in Fig.
 477 7). Additionally, the amount of regeneration is significantly lower for
 478 CO₂/R134a mixture than for pure CO₂ because during the expansion
 479 process CO₂/R134a mixture accommodates a higher pressure drop
 480 and larger enthalpy difference.



481

482 **Fig. 8.** Amount of heat absorption by pure CO₂ and CO₂/R134a
 483 mixture in the PR-ORC.
 484

485 Fig. 9 depicts the relationship between the net power output
 486 estimation and the expansion inlet pressure. As expected, for both
 487 pure CO₂ and CO₂/R134a mixture, the net power output estimations
 488 of the P-ORC and the PR-ORC display upward trend. However,
 489 CO₂/R134a mixture yields more net power output than pure CO₂ in
 490 both the P-ORC and the PR-ORC. The higher net power outputs
 491 achieved by CO₂/R134a mixture are attributed to its lower
 492 condensation pressure and the resulting higher enthalpy difference
 493 in the expansion process. Furthermore, the addition of the
 494 regenerator results in the increase of net power output. In the PR-
 495 ORC system, the maximum net power output of 4.61 kW is achieved
 496 at $P_4=10.7$ MPa for pure CO₂, while 5.30 kW is obtained at
 497 $P_4=10.6$ MPa for CO₂/R134a mixture. Appendix A supplements
 498 detailed experimental results with the thermodynamic properties of
 499 each state point based on maximum net power output.

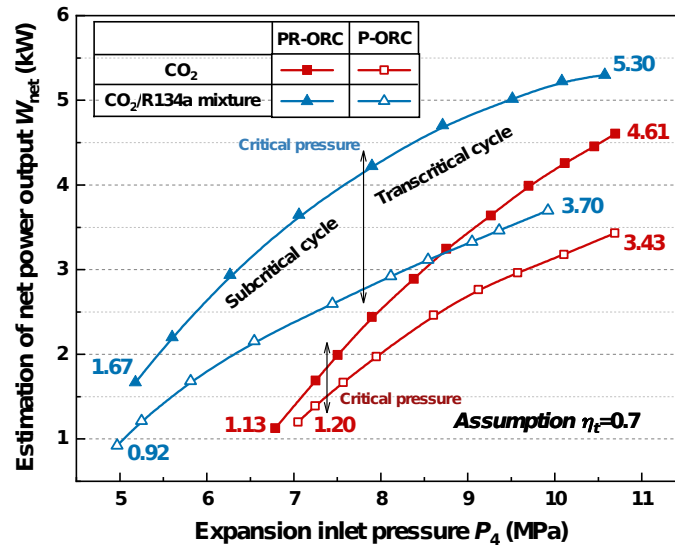


Fig. 9. Estimation of net power output for pure CO₂ and CO₂/R134a mixture in the PR-ORC and the P-ORC.

For a fair comparison, the net power output at a certain expansion inlet pressure value of 10MPa is estimated using a quadratic fitted method based on existing test data. The quadratic fitted results are listed in Table 6. At an expansion inlet pressure of 10MPa, CO₂/R134a provides 16.7% more net power output than pure CO₂ for the P-ORC and 23.3% for the PR-ORC. Including the regenerator, the net power output increases by 32.5% for pure CO₂ and 40% for CO₂/R134a mixture.

Table 6

Fitted results of net power output estimation, thermal efficiency and exergy efficiency at an expansion inlet pressure of 10 MPa.

	CO ₂ /R134a mixture		Pure CO ₂	
	P-ORC	PR-ORC	P-ORC	PR-ORC
Net power output estimation (kW)	3.70	5.18	3.17	4.20
Thermal efficiency (%)	7.45	9.83	5.89	8.44
Exergy efficiency (%)	16.59	23.77	13.82	19.22

500

501

502

503

504

505

506

507

508

509

510

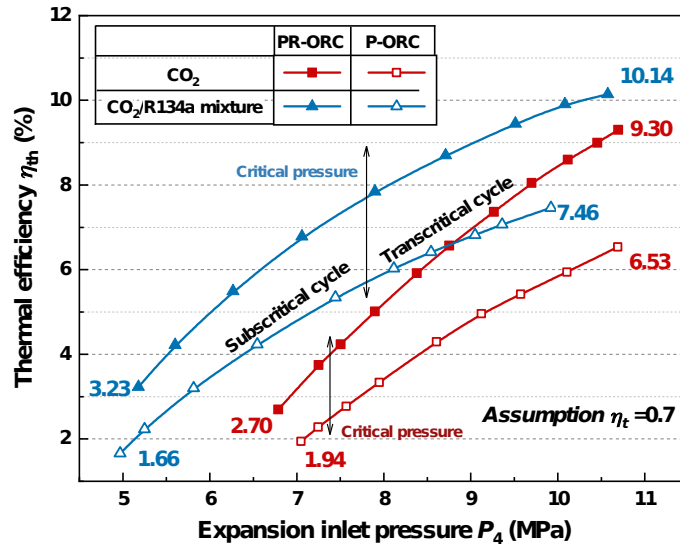
511

512

513

514

515



516

517 **Fig. 10.** Variation in thermal efficiencies for pure CO₂ and
 518 CO₂/R134a mixture in the PR-ORC and the P-ORC.

519

520 Fig. 10 shows the variation in thermal efficiency for pure CO₂
 521 and CO₂/R134a mixture. For all scenarios thermal efficiency shows
 522 an increasing trend with expansion inlet pressure.

523 For system configurations, PR-ORC offers higher thermal
 524 efficiency than P-ORC. Meanwhile, CO₂/R134a mixture is capable of
 525 achieving higher thermal efficiency than pure CO₂ because of its
 526 higher pressure ratio. In the PR-ORC, a maximum thermal efficiency
 527 of 10.14% occurred at $P_4=10.6$ MPa for CO₂/R134a mixture; a
 528 maximum thermal efficiency of 9.30% occurred at $P_4=10.7$ MPa for
 529 pure CO₂. At the same $P_4=10$ MPa shown in Table 6, CO₂/R134a
 530 mixture achieves an increase in thermal efficiency of 26.5% in the P-
 531 ORC and 16.4% in the PR-ORC compared to pure CO₂. Adding the
 532 regenerator increases the thermal efficiency a total by 43.3% for
 533 pure CO₂ and 31.9% for CO₂/R134a mixture.

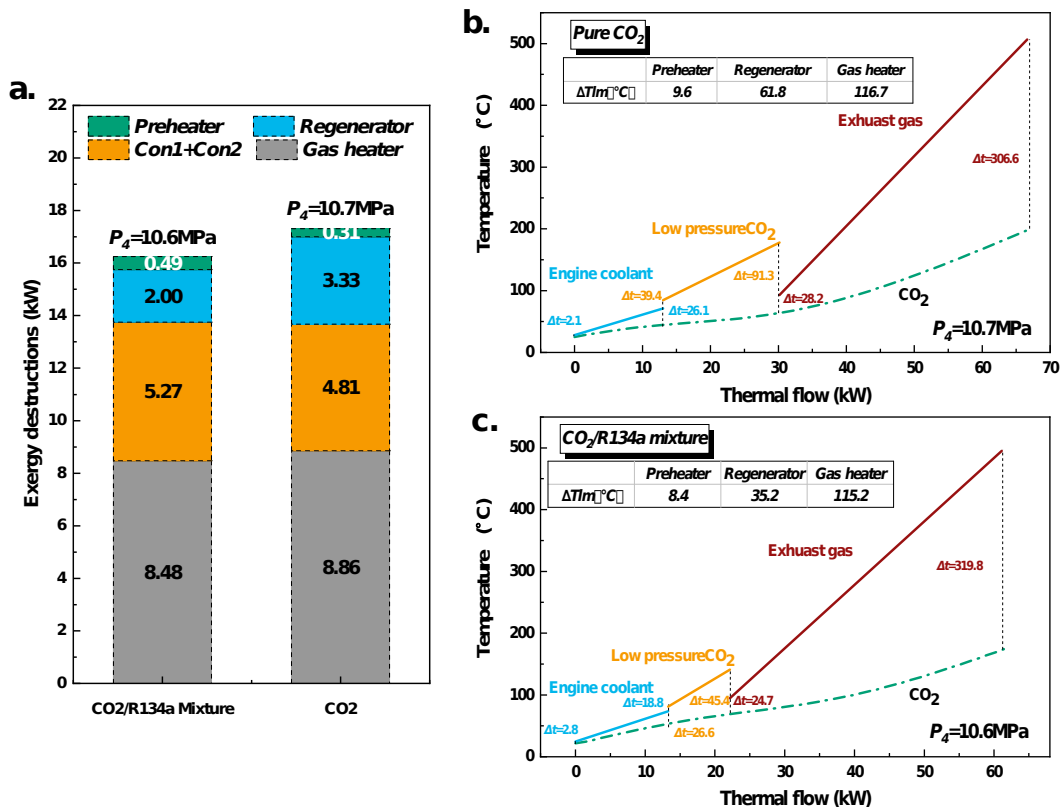
534 Previous studies indicated that CO₂ is capable of achieving a
 535 good thermal matching in the preheater and the a resulting low
 536 exergy destruction [11]. The thermal matching and exergy
 537 destruction of CO₂/R134a mixture is compared with that of pure CO₂
 538 below.

539 Fig.11(a) shows the exergy destructions of various heat
 540 exchangers in the PR-ORC. For both pure CO₂ and CO₂/R134a
 541 mixture, the highest exergy destruction is achieved by the gas
 542 heater, followed by the condenser, the regenerator and the
 543 preheater. Compared to pure CO₂, the CO₂/R134a mixture owns
 544 higher exergy destructions in the condensers but lower exergy
 545 destruction in the gas heater and regenerator. The high exergy
 546 destruction in the condensers may be attributable to the poor

37
 38

547 thermal matching induced by the temperature glide in the
 548 condensing process. Furthermore, the difference of the exergy
 549 destruction in the regenerator and gas heater between pure CO₂
 550 and CO₂/R134a mixture can be explained using Fig.11(b) and
 551 Fig.11(c), in which the log mean temperature differences of heat
 552 exchangers, expressed as ΔT_{lm} , are noted. Clearly, CO₂/R134a
 553 mixture achieves better thermal matching than pure CO₂ in the
 554 regenerator and the gas heater, as reflected by the ΔT_{lm} . The
 555 primary reason for difference in thermal matching is that the peak
 556 specific heat of pure CO₂ is obtained at the temperature range in
 557 which the working fluid absorbs heat from the engine coolant,
 558 whereas the peak specific heat of CO₂/R134a mixture is achieved at
 559 a relatively high temperature (see Fig.7).

560 The maximum exergy efficiencies of pure CO₂ and the
 561 CO₂/R134a mixture are 21.24% and 24.34%, respectively, as shown
 562 in Fig.12. At the $P_4=10$ MPa presented in Table 6, the CO₂/R134a
 563 mixture achieves an increase of 20.0% in the P-ORC and 23.7% in
 564 the PR-ORC compared to pure CO₂. The addition of the regenerator
 565 results in an increase in exergy efficiency of 39.1% for pure CO₂ and
 566 43.3% for the CO₂/R134a mixture.

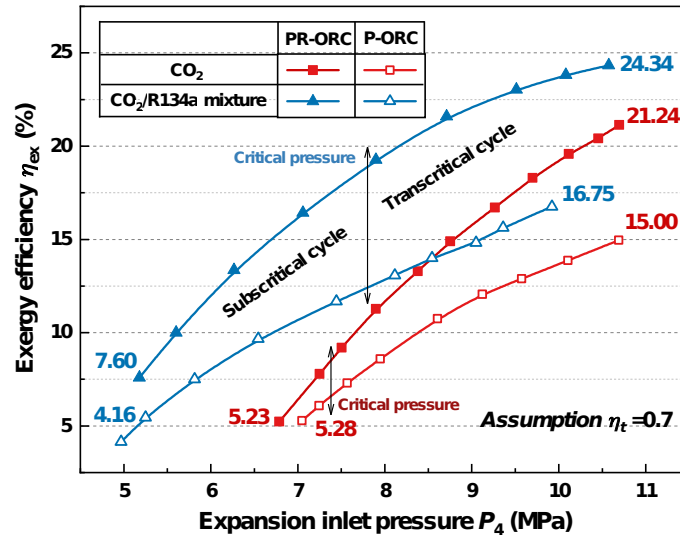


567

568 **Fig. 11.** (a) Exergy destructions of various heat exchangers for pure
 569 CO₂ and CO₂/R134a mixture in the PR-ORC; (b) T - Q plot of heating
 570 process for pure CO₂ ;(c) T - Q plot of heating process for CO₂/R134a

39
 40

571 mixture.



572

573 **Fig. 12.** Variation in exergy efficiencies for pure CO₂ and CO₂/R134a
574 mixture in the PR-ORC and the P-ORC.

575

576 6.3 System performance of CO₂/R134a mixture

577 under ambient cooling conditions.

578 As mentioned above, the low critical temperature of CO₂ makes it
579 difficult for CO₂ to be condensed at ambient cooling sources, which
580 represents the main barrier to using CO₂ for engine waste heat
581 recovery. In this section, the performance of CO₂/R134a mixture was
582 tested further under ambient cooling conditions (25.2~31.5°C).

583 After the refrigerating unit was shut down, the cooling water
584 temperature was increased gradually, as indicated by several
585 parameters, to ensure the steady operation of the ORC system. Fig.
586 13 shows the variation with time of primary measured parameters
587 after shutdown of the refrigerating unit. The cooling water inlet
588 temperature T_{c1} and working fluid temperature at condenser-2 outlet
589 T_8 both rose slowly. The pressure at the condenser-2 outlet P_8
590 increased correspondingly. About 20min after the refrigerating unit
591 shutdown, the temperature of working fluid T_8 reached the critical
592 temperature of 31.1 °C for CO₂. After another 7.5min, the cooling
593 water inlet temperature T_{c1} reached the ambient temperature of 25
594 °C. During this process, P_8 increased from 5.04 to 5.37MPa.

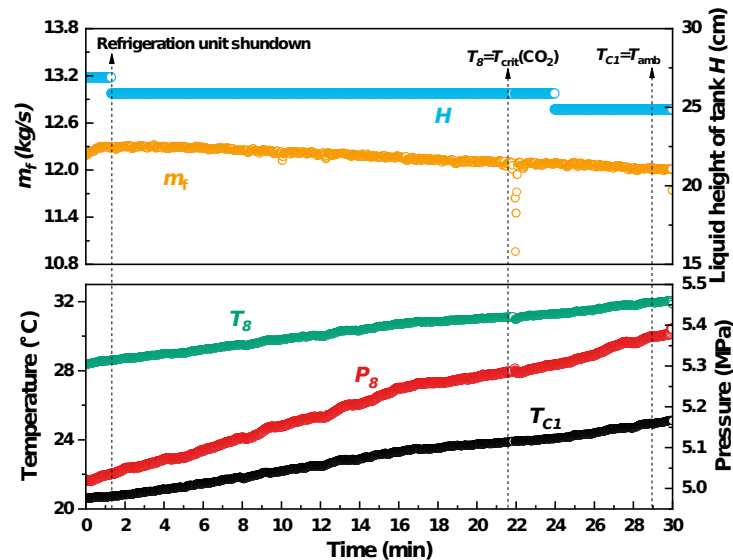
595 The liquid height of working fluid tank H and mass flow rate of
596 working fluid m_f are two important indicators for steady operation of
597 the ORC system. The mass flow rate of the working fluid decreased
598 repositively as cooling water inlet temperature increased. The

599 decreasing trend may be attributable to the decrease in the density
 600 of working fluid at the pump inlet caused by the increase of T_8 . At
 601 about 22min, the system's mass flow rate underwent a sudden
 602 decrease and then a rapid return to a normal value. The fluctuation
 603 in mass flow rate may reflect the fact that the thermos-physical
 604 attributes of CO₂ show drastic and fast changes in the neighborhood
 605 of its critical point.

606 The experimental results described above confirm that an ORC
 607 system using the CO₂/R134a mixture is capable of operating steadily
 608 under ambient cooling conditions, meaning that the CO₂/R134a
 609 mixture can expand the range of condensation temperatures and
 610 alleviate the low-temperature condensation issue encountered with
 611 CO₂. Hence, the CO₂/R134a mixture exhibits a high technical
 612 potential for providing engine waste heat recovery.

613 The experiment under ambient cooling conditions was
 614 performed using the same experimental strategy as described
 615 above. The steady state experimental points used for system
 616 performance estimation are presented in Table 7.

617 Fig. 14 shows the variation in net power output estimations
 618 under ambient cooling conditions. The figure shows that net power
 619 output estimations ranging from 0.42 to 2.88 kW can be obtained by
 620 P-ORC; they vary in the range of 0.66 to 3.54 kW for PR-ORC.
 621

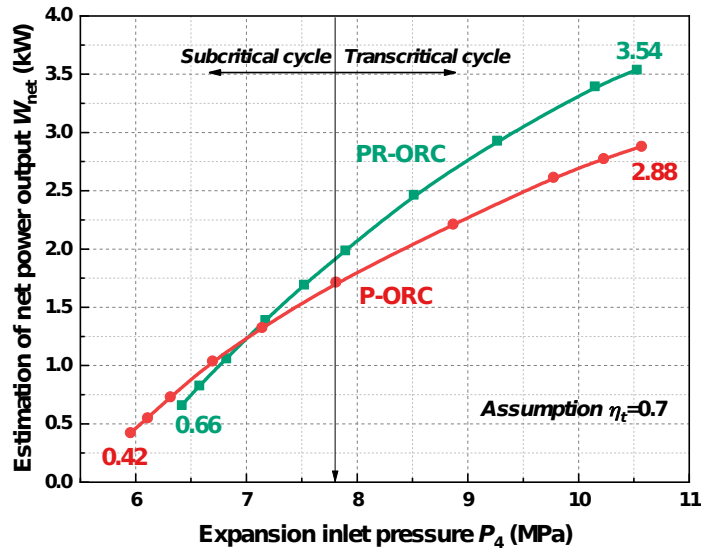


622
 623 **Fig. 13.** Change in primary measured parameters after shutdown of
 624 the refrigerator unit.

625
 626 **Table 7**
 627 Steady state experimental points used for system performance
 628 estimation.

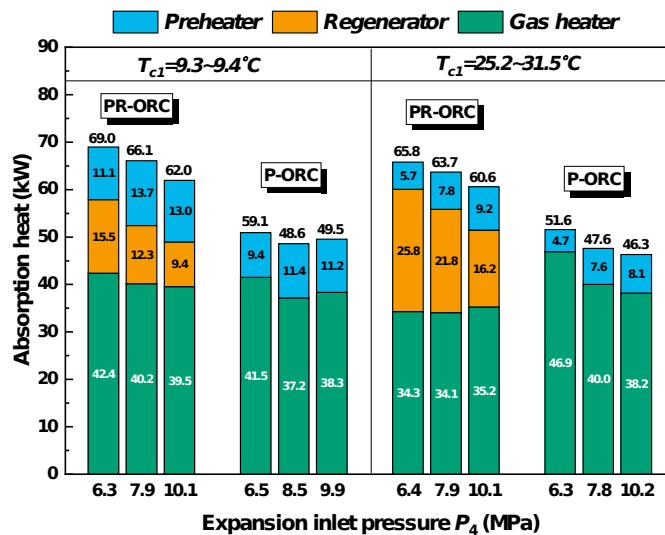
P-ORC										
P_4 /(MPa)	5.95	6.11	6.31	6.70	7.14	7.81	8.87	9.78	10.2	10.5
									3	7
P_5 /(MPa)	5.46	5.49	5.50	5.50	5.50	5.51	5.52	5.51	5.51	5.55
PR-ORC										
P_4 /(MPa)	6.42	6.58	6.82	7.17	7.52	7.90	8.51	9.26	10.1	10.5
									5	3
P_5 /(MPa)	5.82	5.84	5.85	5.88	5.89	5.89	5.91	5.91	5.91	5.93

629



630

631 **Fig. 14.** Variation in net power output under ambient cooling
632 conditions.



633

634 **Fig. 15.** Amount of heat absorption in the P-ORC and the PR-ORC.

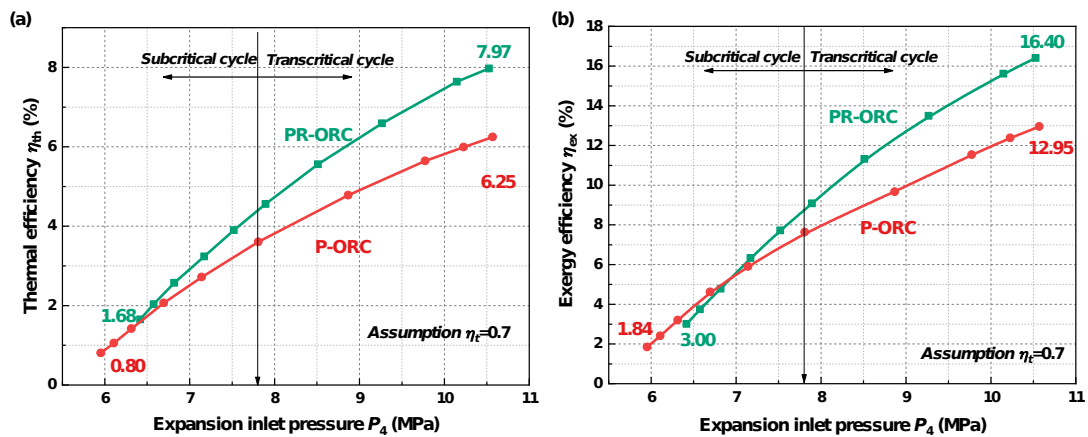
635

636 Fig.14 indicates that PR-ORC provides higher net power output
637 than P-ORC when the expansion inlet pressure exceeds 7.0MPa, a

45

46

638 result that is not realized at a low expansion inlet pressure. This
 639 result is quite different from the abovementioned comparative
 640 experimental results with pure CO₂. The lower net power obtained
 641 by the PR-ORC at low pressure is attributed to the decrease in heat
 642 absorption as depicted in Fig.15. The increase in the expansion
 643 outlet pressure leads to a decrease of the pressure ratio and a
 644 resulting higher expansion outlet temperature. Thus, the PR-ORC
 645 system absorbs more heat in the regenerator while withdrawing less
 646 heat from exhaust gas. The high expansion outlet pressure also
 647 reduces the amount of heat absorption in the preheater.



648 **Fig. 16.** Performance of the P-ORC and the PR-ORC: (a) thermal
 649 efficiency; (b) exergy efficiency.
 650
 651

648
 649
 650
 651
 652
 653
 654
 655
 656
 657
 658
 659
 660
 661

Fig.16 shows the thermal efficiency and exergy efficiency of both the P-ORC and the PR-ORC. The trend in thermal efficiency is a combination of the net power output estimation and the amount of heat absorption, as discussed above. The maximum thermal efficiency of the PR-ORC is 7.97%, achieved at $P_4=10.5$ MPa. Maximum thermal efficiency of the P-ORC is 6.25% at 10.6MPa. The exergy efficiency shown in Fig.16(b) shows the same trend as the net power output, which means the net power output is critical in influencing the exergy efficiency. The maximum exergy efficiencies of the PR-ORC and the P-ORC are 16.40% and 12.95%, respectively.

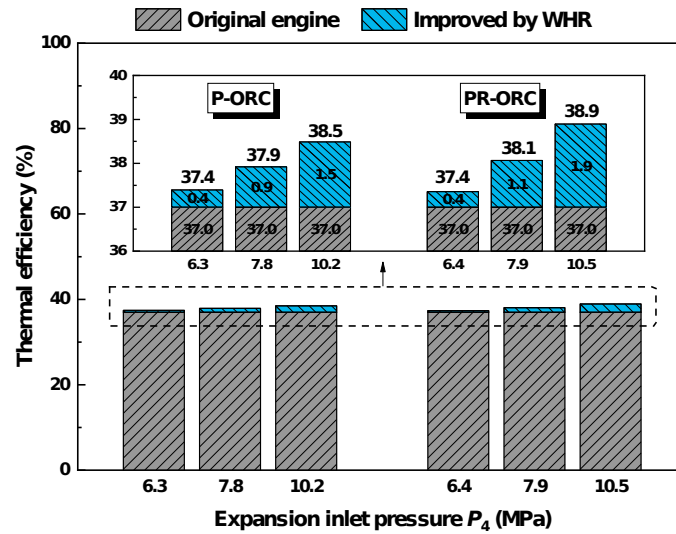


Fig. 17. Thermal efficiency of diesel engine and combined diesel engine -ORC combined system.

Combined with the ORC system, the thermal efficiency of the diesel engine would be improved. The thermal efficiencies of the original diesel engine and the diesel engine combined with the ORC system are depicted in Fig.17. given an ambient cooling source, the maximum improvement in thermal efficiency is 1.5% for the P-ORC and 1.9% for the PR-ORC. Hence, the thermal efficiency of the combined diesel engine-ORC system can reach 38.9% versus an original diesel engine thermal efficiency of 37%.

7. Conclusion

A preliminary experimental comparison of pure CO_2 and a $\text{CO}_2/\text{R134a}$ mixture (0.6/0.4 on a mass basis) for engine waste heat recovery was performed using an expansion valve. Measured operating parameters and system performance were compared under the preheating Organic Rankine Cycle (P-ORC) and the preheating regenerative Organic Rankine Cycle (PR-ORC). In addition, the application potential of $\text{CO}_2/\text{R134a}$ (0.6/0.4) mixture for engine waste heat recovery was tested under ambient cooling conditions. The primary conclusions of this work are given below.

- (1) For the PR-ORC, as the expansion inlet pressure increases, the expansion inlet temperature increases from 181.6°C to about 200°C for CO_2 , while the expansion inlet temperature of $\text{CO}_2/\text{R134a}$ mixture decreases from 188.5°C to 175.2°C .
- (2) $\text{CO}_2/\text{R134a}$ (0.6/0.4) mixture exhibits better system performance than pure CO_2 . For the PR-ORC using $\text{CO}_2/\text{R134a}$ (0.6/0.4) mixture, assuming a turbine isentropic efficiency of 0.7, the net power output estimation, thermal efficiency and

692 exergy efficiency reach 5.30kW, 10.14% and 24.34%,
693 respectively. At the same expansion inlet pressure of 10MPa,
694 the net power output estimation, thermal efficiency and
695 exergy efficiency using CO₂/R134a mixture achieve an
696 increase of 23.3%, 16.4% and 23.7%, respectively, compared
697 with using pure CO₂ as working fluid.

698 (3)The PR-ORC performs better than the P-ORC for both pure
699 CO₂ and CO₂/R134a mixture. By adding the regenerator for
700 the case of CO₂/R134a (0.6/0.4) mixture, net power output
701 estimation, thermal efficiency and exergy efficiency increase
702 by 40%, 31.9% and 43.3%, respectively.

703 (4)In the heating process, CO₂/R134a (0.6/0.4) mixture shows
704 better thermal matching in the regenerator and the gas
705 heater compared with pure CO₂. We attribute this result to
706 the its high temperature range for the peak specific heat.
707 CO₂/R134a (0.6/0.4) mixture demonstrates poor thermal
708 matching in the cooling process because of its temperature
709 glide.

710 (5)Experiments showed that the ORC system using CO₂/R134a
711 mixture (0.6/0.4) is capable of operating steadily under
712 ambient cooling conditions. Results demonstrates that
713 CO₂/R134a mixture can expand the range of condensation
714 temperature and thus alleviate the low-temperature
715 condensation issue encountered with CO₂. Under ambient
716 cooling conditions, the thermal efficiency of a diesel engine is
717 expected to be improved by 1.9% using CO₂/R134a (0.6/0.4)
718 mixture.

719 **Acknowledgement**

720 The authors would like to acknowledge the Key Technologies
721 Research and Development Program of China (2017YFE0102800) for
722 grants and supports. Financial support from China Scholarship
723 Council (CSC) to the first author also is gratefully acknowledged.

724 The U.S. authors recognize Lawrence Berkeley National
725 Laboratory's support from Department of Energy - The United
726 States under Contract No. DE-AC02-05CH11231 and supports from
727 the Energy Foundation. The U.S. Government retains a non-
728 exclusive, paid-up, irrevocable, world-wide license to publish or
729 reproduce the published form of this manuscript, or allow others to
730 do so, for U.S. Government purposes.

731 **Appendix A**

732 Detailed experimental results along with the thermodynamic
733 properties of each state point based on maximum net power output.

Point	T/(°C)	P/(MPa)	h/(kJ/kg)	s/(kJ/kg K)
Pure CO₂				
1	25.9	10.74	257.2	1.1709
2	41.1	10.73	309.6	1.3416
3	64.9	10.71	426.8	1.7028
4	200.0	10.69	629.9	2.2194
5	178.0	5.98	622.8	2.3053
6	84.6	5.95	516.3	2.0410
7	21.3	5.94	260.1	1.2013
8	21.0	5.93	258.9	1.1971
9	19.3	5.93	251.9	1.1734
CO₂/R134a mixture				
1	21.9	10.64	238.7	1.1081
2	44.6	10.61	285.2	1.2602
3	70.0	10.62	357.2	1.4774
4	175.2	10.57	566.2	2.0234
5	141.0	3.96	559.8	2.1333
6	81.3	3.93	492.5	1.9587
7	23.9	3.92	310.8	1.3773
8	17.1	3.90	233.8	1.1153
9	16.3	3.90	232.1	1.1094

734

735 References

- 736 [1]. International Energy Agency, World Energy Outlook 2017.
737 2017.11. <https://www.iea.org/weo2017/>.
- 738 [2]. Shu, G, G Yu, H Tian, H Wei, X Liang,Z Huang. Multi-approach
739 evaluations of a cascade-Organic Rankine Cycle (C-ORC)
740 system driven by diesel engine waste heat: Part A -
741 Thermodynamic evaluations. Energy Conversion and
742 Management 2016. 108:579-595.
- 743 [3]. Villani, M,L Tribioli. Comparison of different layouts for the
744 integration of an organic Rankine cycle unit in electrified
745 powertrains of heavy duty Diesel trucks. Energy Conversion
746 and Management 2019. 187:248-261.
- 747 [4]. Yang, M-H. Payback period investigation of the organic
748 Rankine cycle with mixed working fluids to recover waste heat
749 from the exhaust gas of a large marine diesel engine. Energy
750 Conversion and Management 2018. 162:189-202.
- 751 [5]. Soffiato, M, CA Frangopoulos, G Manente, S Rech,A Lazzaretto.
752 Design optimization of ORC systems for waste heat recovery
753 on board a LNG carrier. Energy Conversion and Management

- 754 2015. 92:523-534.
- 755 [6]. Wang, X, G Shu, H Tian, W Feng, P Liu, X Li. Effect factors of
756 part-load performance for various Organic Rankine cycles
757 using in engine waste heat recovery. Energy Conversion and
758 Management 2018. 174:504-515.
- 759 [7]. Harby, K. Hydrocarbons and their mixtures as alternatives to
760 environmental unfriendly halogenated refrigerants: An
761 updated overview. Renewable & Sustainable Energy Reviews
762 2017. 73:1247-1264.
- 763 [8]. UNEP. Handbook for international treaties for protection of the
764 ozone layers. 6th ed. United Nation Environment Program
765 (UNEP). Nairobi, Kenya 2003.
- 766 [9]. Shu, G, L Shi, H Tian, X Li, G Huang, L Chang. An improved
767 CO₂-based transcritical Rankine cycle (CTRC) used for engine
768 waste heat recovery. Applied Energy 2016. 176:171-182.
- 769 [10]. Shu, G, L Shi, H Tian, S Deng, X Li, L Chang. Configurations
770 selection maps of CO₂-based transcritical Rankine cycle
771 (CTRC) for thermal energy management of engine waste heat.
772 Applied Energy 2016.
- 773 [11]. Shi, L, G Shu, H Tian, G Huang, T Chen, X Li, et al.
774 Experimental comparison between four CO₂-based
775 transcritical Rankine cycle (CTRC) systems for engine waste
776 heat recovery. Energy Conversion and Management 2017.
777 150:159-171.
- 778 [12]. Song, J, X-s Li, X-d Ren, C-w Gu. Performance improvement of a
779 preheating supercritical CO₂ (S-CO₂) cycle based system for
780 engine waste heat recovery. Energy Conversion and
781 Management 2018. 161:225-233.
- 782 [13]. Irwin, L, Y Le Moullec. Turbines can use CO₂ to
783 cut CO₂. Science 2017. 356;(6340):805-806.
- 784 [14]. Musgrove., G O, D Shiferaw., S Sullivan., LCM Portnoff. Tutorial:
785 Heat Exchangers for Supercritical CO₂ Power Cycle
786 Applications,. 2016.
- 787 [15]. Choi, BC. Thermodynamic analysis of a transcritical CO₂ heat
788 recovery system with 2-stage reheat applied to cooling water
789 of internal combustion engine for propulsion of the 6800 TEU
790 container ship. Energy 2016. 107:532-541.
- 791 [16]. Wang, SS, C Wu, J Li. Exergoeconomic analysis and
792 optimization of single-pressure single-stage and multi-stage
793 CO₂ transcritical power cycles for engine waste heat recovery:
794 A comparative study. Energy 2018. 142:559-577.
- 795 [17]. Persichilli, M, T Held, S Hostler, E Zdankiewicz, D Klapp.
796 Transforming waste heat to power through development of a
797 CO₂-based-power cycle. Electric Power Expo 2011:10-12.

- 798 [18]. Li, X, G Shu, H Tian, L Shi, G Huang, T Chen, et al. Preliminary
799 tests on dynamic characteristics of a CO₂ transcritical power
800 cycle using an expansion valve in engine waste heat recovery.
801 Energy 2017. 140:696-707.
- 802 [19]. Shi, L, G Shu, H Tian, T Chen, P Liu, L Li. Dynamic tests of CO₂-
803 Based waste heat recovery system with preheating process.
804 Energy 2019. 171:270-283.
- 805 [20]. Li, X, G Shu, H Tian, G Huang, P Liu, X Wang, et al.
806 Experimental comparison of dynamic responses of
807 CO₂ transcritical power cycle systems used for
808 engine waste heat recovery. Energy Conversion and
809 Management 2018. 161:254-265.
- 810 [21]. Garg, P, P Kumar, K Srinivasan, P Dutta. Evaluation of carbon
811 dioxide blends with isopentane and propane as working fluids
812 for organic Rankine cycles. Applied Thermal Engineering 2013.
813 52;(2):439-448.
- 814 [22]. Shu, G, Z Yu, H Tian, P Liu, Z Xu. Potential of the transcritical
815 Rankine cycle using CO₂-based binary zeotropic mixtures for
816 engine's waste heat recovery. Energy Conversion and
817 Management 2018. 174:668-685.
- 818 [23]. Dai, B, M Li, Y Ma. Thermodynamic analysis of carbon dioxide
819 blends with low GWP (global warming potential) working
820 fluids-based transcritical Rankine cycles for low-grade heat
821 energy recovery. Energy 2014. 64;(1):942-952.
- 822 [24]. Wu, C, S S Wang, X Jiang, J Li. Thermodynamic analysis and
823 performance optimization of transcritical power cycles using
824 CO₂-based binary zeotropic mixtures as working fluids for
825 geothermal power plants. Applied Thermal Engineering 2017.
826 115:292-304.
- 827 [25]. Pan, L, X Wei, W Shi. Performance analysis of a zeotropic
828 mixture (R290/CO₂) for trans-critical power cycle. Chinese
829 Journal of Chemical Engineering 2015. 23;(3):572-577.
- 830 [26]. Yin, H, A S Sabau, J C Conklin, J McFarlane, A L Qualls. Mixtures of
831 SF₆-CO₂ as working fluids for geothermal power plants ☆.
832 Applied Energy 2013. 106;(11):243-253.
- 833 [27]. Bamorovat Abadi, G, K C Kim. Investigation of organic Rankine
834 cycles with zeotropic mixtures as a working fluid: Advantages
835 and issues. Renewable and Sustainable Energy Reviews 2017.
836 73:1000-1013.
- 837 [28]. Wang, J L, L Zhao, X D Wang. A comparative study of pure and
838 zeotropic mixtures in low-temperature solar Rankine cycle.
839 Applied Energy 2010. 87;(11):3366-3373.
- 840 [29]. Bamorovat Abadi, G, E Yun, K C Kim. Experimental study of a
841 1 kw organic Rankine cycle with a zeotropic mixture of

842 R245fa/R134a. Energy 2015. 93:2363-2373.

843 [30]. Jung, HC, L Taylor,S Krumdieck. An experimental and
844 modelling study of a 1kW organic Rankine cycle unit with
845 mixture working fluid. Energy 2015. 81:601-614.

846 [31]. Li, T, J Zhu, W Fu,K Hu. Experimental comparison of R245fa
847 and R245fa/R601a for organic Rankine cycle using scroll
848 expander. International Journal of Energy Research 2015. 39;
849 (2):202-214.

850 [32]. Pang, K-C, S-C Chen, T-C Hung, Y-Q Feng, S-C Yang, K-W Wong,
851 et al. Experimental study on organic Rankine cycle utilizing
852 R245fa, R123 and their mixtures to investigate the maximum
853 power generation from low-grade heat. Energy 2017. 133:636-
854 651.

855 [33]. Meng, Z, H Zhang, M Lei, Y Qin,J Qiu. Performance of low GWP
856 R1234yf/R134a mixture asa replacement for R134a in
857 automotive air conditioning systems. International Journal of
858 Heat and Mass Transfer 2018. 116:362-370.

859 [34]. Uusitalo, A, J Honkatukia,T Turunen-Saaresti. Evaluation of a
860 small-scale waste heat recovery organic Rankine cycle.
861 Applied Energy 2017. 192:146-158.

862 [35]. Brun, K, P Friedman,R Dennis, Fundamentals and applications
863 of supercritical carbon dioxide (sCO₂) based power cycles.
864 2017: Woodhead publishing.

865

Nomenclature			
c_p	Specific heat (kJ/kW K)	is	Isentropic
E	Exergy flow rate (kW)	in	Inlet
h	Enthalpy (kJ/kg)	max	Maximum
I	Exergy destruction (kW)	net	Net power
m	Mass flow rate (kg/s)	out	Outlet
P	Pressure (MPa)	p	Pump
Q	Heat flow rate (kW)	pre	Preheater
T	Temperature (°C)	reg	Regenerator
W	Power output (kW)	t	Turbine
η	Efficiency (%)	th	Thermal
ΔT_{lm}	Log mean temperature difference(°C)		
Subscripts		Abbreviations	
con	Condenser	CW	Cooling water

<i>cw</i>	Cooling water side	EC	Engine coolant
<i>1-9</i>	Work fluid state point	EG	Exhaust gas
<i>ave</i>	Average	ICE	Internal combustion engine
<i>eg</i>	Exhaust gas side	ORC	Organic Rankine Cycle
<i>ex</i>	Exergy	P-ORC	Preheating Organic Rankine Cycle
<i>exp</i>	Expansion process	PR-ORC	Preheating regenerative Organic Rankine Cycle
<i>est</i>	Estimation	PR	Pressure ratio
<i>f</i>	Working fluid	RD	Relative difference
<i>gh</i>	Gas heater	WHR	Waste heat recovery

866